Enhanced thermodynamic modelling of a gamma-type stirling engine

Alfarawi, Suliman; Al-Dadah, Raya; Mahmoud, Saad

DOI:
10.1016/j.applthermaleng.2016.06.145

Document Version
Peer reviewed version

Citation for published version (Harvard):
Alfarawi, S, Al-Dadah, R & Mahmoud, S 2016, 'Enhanced thermodynamic modelling of a gamma-type stirling engine', Applied Thermal Engineering, vol. 106, pp. 1380-1390.
https://doi.org/10.1016/j.applthermaleng.2016.06.145

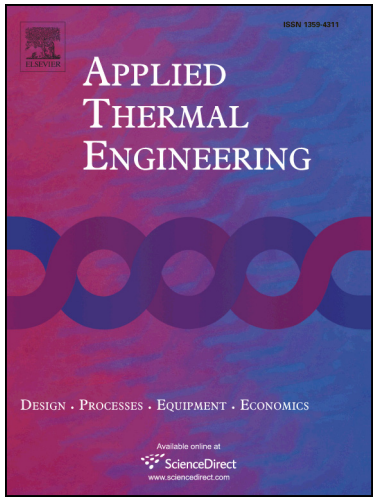

Enhanced thermodynamic modelling of a gamma-type stirling engine

S. Alfarawi, R. AL-Dadah, S. Mahmoud

PII: S1359-4311(16)31058-4
DOI: http://dx.doi.org/10.1016/j.applthermaleng.2016.06.145
Reference: ATE 8556

To appear in: *Applied Thermal Engineering*

Received Date: 2 April 2016
Revised Date: 8 June 2016
Accepted Date: 21 June 2016

Please cite this article as: S. Alfarawi, R. AL-Dadah, S. Mahmoud, Enhanced thermodynamic modelling of a gamma-type stirling engine, *Applied Thermal Engineering* (2016), doi: http://dx.doi.org/10.1016/j.applthermaleng.2016.06.145

Revised manuscript

ENHANCED THERMODYNAMIC MODELLING OF A GAMMA-TYPE STIRLING ENGINE

S. Alfarawi[1], R. AL-Dadah[1], S. Mahmoud[1]

[1] *Department of Mechanical Engineering, University of Birmingham, Edgbaston, B15 2TT, UK*

Abstract

Modelling can substantially contribute to the development of Stirling engines technology and help understanding the fundamental processes of the real cycle for further performance improvement. In the present work, an enhanced thermodynamic model for Gamma-type Stirling engine simulation was developed based on the reconfiguration of non-ideal adiabatic analysis**.** The developed model was validated against experimental measurements on Stirling engine prototype (ST05 CNC), available at University of Birmingham. Good agreement was found between the model and experiment in predicting the indicated power, shaft power and thermal efficiency at different operating conditions. A parametric study was carried out to investigate the effect of phase angle, gas type, regenerator matrix type and dead volume on engine performance. The feasibility of utilizing the stored cold energy of LN2 to maximize the shaft power was also presented. Results showed that shaft power can be significantly enhanced by 49% for helium and 35% for nitrogen when cooling temperature is lowered to -50 °C while heating temperature remains constant at 650°C.

Keywords: Enhanced, Thermodynamic, Modelling, Simulation, Gamma-type, Stirling Engine

Nomenclature

A_f	Internal wetted area (m^2)	$Q_{sh,loss}$	Shuttle heat loss (J)
A_h	Heater internal wetted area (m^2)	R	Gas constant (J/kg. K)
A_{k1}	Connecting pipe internal wetted area (m^2)	r	Crank radius (m)
A_{k2}	Cooler internal wetted area (m^2)	Re	Reynolds number
A_r	Regenerator internal wetted area (m^2)	T_h	Ideal heater gas temperature (K)
C_p	Gas heat capacity at constant pressure (J/kg. K)	T_k	Ideal cooler gas temperature (K)
C_v	Gas heat capacity at constant volume (J/kg. K)	T_r	Ideal regenerator gas temperature (K)
CVC	Compression clearance volumes (m^3)	T_e	Expansion space temperature (K)
CVE	Expansion clearance volumes (m^3)	T_c	Compression space temperature (K)
D_d	Displacer diameter (m)	T_{he}	Conditional temperature expansion cell / heater (K)
d_r	Regenerator hydraulic diameter (m)	T_{ck1}	Conditional temperature compression cell / pipe (K)

E	Mechanism effectiveness	T_{wh}	Heater wall temperature (K)
f_D	Darcy friction factor	T_{wk}	Cooler wall temperature (K)
f_r	Reynolds friction factor	T_{gh}	Ideal heater gas temperature (K)
h_h	Heater heat transfer coefficient (W/m^2. K)	T_{gk}	Ideal cooler gas temperature (K)
h_{k1}	Pipe heat transfer coefficient (W/m^2. K)	u	Gas velocity (m/s)
h_{k2}	Cooler transfer coefficient (W/m^2. K)	V_c	Compression volume variation, (m^3)
J	Colburn J-factor	V_e	Expansion volume variation, (m^3)
J_d	Displacer annular gap (m)	V_{k1}	Connecting pipe void volume (m^3)
k	Gas thermal conductivity (W/m. K)	V_{k2}	Cooler void volume (m^3)
k_d	Displacer thermal conductivity (W/m. K)	V_r	Regenerator void volume (m^3)
k_r	Regenerator thermal conductivity (W/m. K)	V_{SC}	Compression swept volumes (m^3)
l_r	Regenerator effective length (m)	V_{SE}	Expansion swept volumes (m^3)
m	Total mass of gas (kg)	$\bar{W}$	Forced work (W)
$\dot{m}$	Mass flow rate (kg/s)	W_{loss}	Pumping loss (W)
n	Engine speed (rpm)	$\dot{W}_s$	Shaft power (W)
NTU	Number of transfer units	W_s	Shaft work (J)
N_u	Nusselt number	X_c	Displacer piston displacement (m)
p	Instantaneous gas pressure, Pa	X_e	Power piston displacement (m)
p_{ch}	Charge pressure, Pa	Z_d	Displacer stroke (m)
P_e	Peclet number	*Greek letter*	
P_r	Prandtle number	ε	Porosity
$Q_{act,h}$	Actual heat transferred to heater (J)	ω	Angular velocity (rad/s)
$Q_{d,loss}$	Conduction heat loss (J)	γ	Specific heat ratios
Q_h	Heat transferred to heater (J)	θ	Crank angle, rad
Q_k	Heat transferred to cooler (J)	μ	Absolute gas viscosity (Pa. s)
Q_r	Heat transferred to regenerator (J)	λ_e	Crank radius to expansion connecting rod ratio
$Q_{r,loss}$	Regenerator heat loss (J)	λ_c	Crank radius to compression connecting rod ratio
$Q_{r,max}$	Maximum regenerator heat loss (J)	ρ	Gas density (kg/m^3)
$Q_{r,min}$	Minimum regenerator heat loss (J)		

1. Introduction

Alternative sources of energy are being sought to preserve fossil fuels as well as to reduce the greenhouse effects. In this regard, renewable energy resources (such as biomass, solar, geothermal and wind energy) are deemed to be the promising solution in as much as they are clean, efficient, and sustainable [1].

Recently, there has been a revival of attention by researchers and developers towards Stirling engines as they are externally heated engines, thermally regenerative, simple in construction, virtually quiet, safe in operation, and intrinsically flexible to adopt any heat source such as solar, biomass, geothermal energy or even an industrial waste [2].

Ideally, Stirling engines work on a highly efficient thermodynamic cycle. The gas inside the engine undergoes four processes; two isothermal heat-exchange processes (expansion and compression) and two isochoric heat-exchange processes (heating and cooling). However, the real cycle is considerably

penalized due to the irreversibility and non-ideality of transport mechanisms occurring inside the different components of the engine.

Stirling engines are mechanically arranged into three configurations, as shown in figure 1, namely, alpha, beta and gamma. For all of the three configurations, the cycle is thermodynamically similar. In alpha Stirling, hot and cold pistons mounted in separate cylinders placed on each side of the regenerator. The V arrangement and the yoke drive (Ross linkage) are often applied to this type of engine.

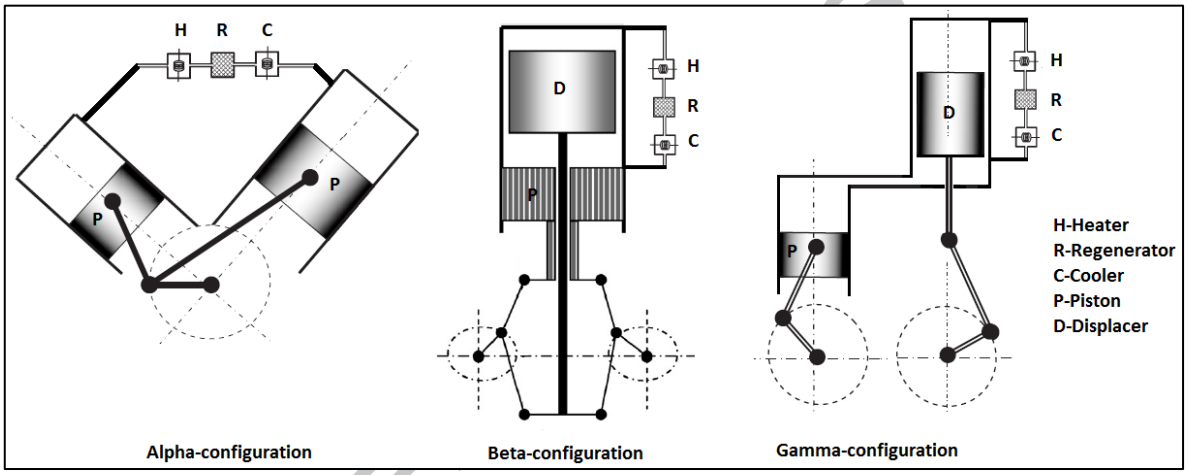

Figure 1: Schematic diagram of Stirling engine arrangements.

The beta Stirling consists of power piston and displacer incorporated in the same cylinder. One mechanical disadvantage is that a drive rod from the displacer extends through the piston. On the other hand, higher compression, efficiency, and power can be obtained due to lower dead volume. The rhombic drive is often applied to this type of engine.

In gamma Stirling, the power piston and displacer are located in separate cylinders. The power piston, which is located at the cold side of the cylinder, compresses or expands the gas being pushed into the cylinder. This configuration of the engine is mechanically more efficient than the others [3]. However, it has higher dead volumes specifically the connecting pipe that connects both the compression space and the lower part of the expansion space. The standard crank drive is often applied to this type of engine.

The regenerator is a key component of the engine, it is an internal heat exchanger that acts as a thermal sponge that absorbs and releases heat during the cycle, thus, enhancing engine power and efficiency. The heat being absorbed and restored to the gas in the regenerator during one cycle is typically four times the heat that passes through the heater during one cycle [4].

Without a regenerator, such an engine requires a heater with five times the amount of heat needed to generate the same power it did with a regenerator. The conventional regenerator types adopted in Stirling engines are wire mesh or random fibre. Some advantageous features exist in the wire matrix such as; high convective heat transfer between the solid and the gas due to the extended surface area of wires and this is similar to a cross flow over repeated cylinder-shaped wires and low axial conduction in flow direction

However, the disadvantage of this type of regenerator is the high flow friction resulting from flow separation, eddies associated with stagnation areas that can degrade the engine performance. The regenerator has to have several features for better performance that might be contradicting and this requires a great effort for designers and developers to find the optimum configuration based on; minimum pressure drop, maximum convective heat transfer and minimum axial conduction in flow direction [5].

There have been numerous numerical models in open literature to analyse and optimize Stirling engines. In their hierarchal order, they are classified as zeroth-, first-, second-, third- and forth- order models. Zero order analysis is based on an empirical correlation to predict the power output of an engine. Beale [6] proposed a correlation based on extensive experimental work of certain layouts of Stirling engines. Later, West [7], developed this approach to predict the power output, using a generalized Beale number at different operational parameters.

The first order analysis was first introduced by Schmidt [8] who developed a closed-form analytical approach to predict the engine power for the case of sinusoidal volume variation based on the assumption of isothermal working spaces. Usually, the power and efficiency predicted by Schmidt analysis, are overestimated by a margin of 30% or even more [9].

Urielli and Berchowitz [10], improved the modelling accuracy further by developing the non-ideal adiabatic analysis. The engine is simplified into five cell units including the three heat exchangers (heater, cooler and regenerator), with the assumption that both expansion and compression spaces are adiabatic.

This implies evaluating and subtracting power and thermal losses from ideal cycle analysis. This approach is widely used as it is fast and returns a reasonably accurate results within a 20% of deviation.

The third order analysis proposed by Finkelstein [11], is a nodal analysis which includes applying the conservation of mass, momentum and energy at nodal points of the engine. This approach adds more complexity by coupling different energy losses into the governing equations. Therefore, this model may not be suitable for optimization purposes due to the increased computational time. The fourth-order analysis or namely computational fluid dynamics (CFD) analysis can return accurate results of engine performance predictions. However, this approach is quite challenging and computationally expensive to model the engine as a whole.

Martini [12] published experimental data on a beta-type Stirling engine (GPU3), which is widely referenced in literature for the validation of analysis methods. Timoumi [13] developed a model for GPU3 based on a second- order analysis with a deviation of 15%. He considered different losses in the model such as shuttle losses, flow resistance, heat conduction losses and hysteresis gas losses. Cheng [14] developed a non-ideal adiabatic model for a domestic-scale 300-W Stirling engine with 20% deviation when compared to experimental results. He investigated the effect of wire mesh number on engine performance and an optimum value was found.

Recent researchers, [15,16,17] incorporated finite speed thermodynamics with adiabatic analysis or polytrophic analysis with deviation of 16% from experimental results. However, most previous works relied on validating models based on a limited experimental data such as comparing with indicated power alone or shaft power alone. Without extensive experimental data, it is hard to develop a reliable thermodynamic model for further understanding of the real cycle.

Modelling gamma-type Stirling engines with non-ideal adiabatic analysis was widely reported in literature. However, in all previous models, the connecting pipe that connects both the lower part of the expansion space and the compression space is always omitted from analysis. This dead volume (connecting pipe) is higher in this type of engine compared to other engine configurations. Therefore, the gas mass that transfers from the compression cell to the cooler back and forth is not correctly computed and hence the heat exchange in other spaces of the engine, based on Reynolds number, is under-

estimated. On the other hand, this causes a deviation in minimum and maximum cyclic pressures and hence a deviation between the calculated average cyclic pressure from the model simulation and the predefined charge pressure.

In this work, the development and validation of an enhanced thermodynamic model based on non-ideal adiabatic analysis for gamma-type Stirling engine is presented. Modelling the engine is reconfigured with six engine cells to include the connecting pipe into the analysis. Random fibre correlations for flow friction and heat transfer, based on oscillatory flow testing, are adopted to model the regenerator. The real pistons motion is adopted and hence the real volume variation is included in the model. The pumping losses in the heat exchangers are evaluated depending on the type of flow regime. Meanwhile, thermal losses such as shuttle and conduction losses are accounted for. Moreover, mechanical losses are also included to predict the shaft power.

2. Engine Description

The engine is a gamma-type that was first designed by Dieter Viebach in 1992 in Germany to promote microgeneration with biomass fuels and since then was opened for research development [18]. The engine, shown in figure 2, is instrumented with eight k-type thermocouples fitted in different locations of the engine for local temperature measurements; compression space, cooling water inlet, cooling water outlet, cooler working gas, regenerator cold end, regenerator hot end, heater working gas and heater wall. High-pressure sensor fitted in the compression space, for instantaneous pressure measurements and dynamometer for brake power measurement. The engine operational details are summarized in table 1. Uncertainty analysis is performed on engine measured parameters using the method presented in [19], and the results are tabulated in table 2. All sources of uncertainties may be linked to the inaccuracies of sensors, data acquisition system, junctions and electrical disturbance. The highest uncertainty, 2.87%, is recorded for the thermal efficiency due to the relative uncertainties in measuring cooling water flow rate, inlet water cooling temperature, outlet water cooling temperature and shaft power.

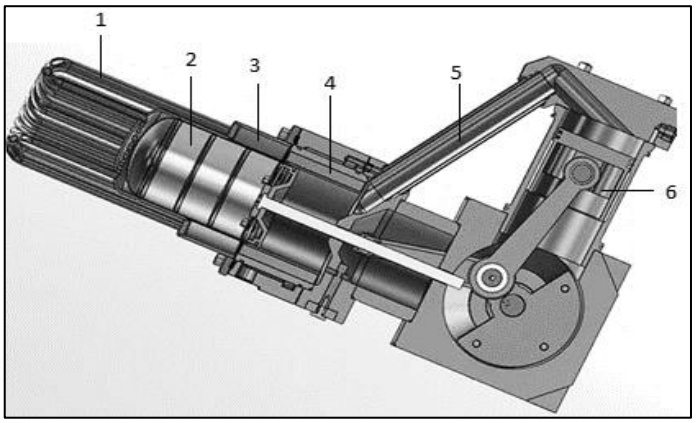

Figure 2: Engine components: 1- Heater, 2- Displacer piston, 3- Regenerator, 4-Cooler, 5-Connecting pipe, 6-Power piston.

Table 1: Engine details.

Parameter	Value
Nominal rotational speed (rpm)	500
Stroke (mm)	75
Power piston bore (mm)	85
Displacer piston bore (mm)	96
Charge pressure (bar)	10
Working gas	N2
Heater type	Tubular
Cooler type	Finned water jacket
Regenerator type	Random fibre
Wire diameter (Micron)	31
Porosity	0.9
Hot source temperature (°C)	650
Inlet water temperature (°C)	15
Water flow rate (L/min)	3.5
Water cooling power (kW)	2.3
Compression ratio	1.3

Table 2: Uncertainty analysis for measured parameters.

Device	Manufacturer	Measurement	Full Scale	Accuracy	Uncertainty
Torque-gauge	Lorenz	Torque	1-50 N.m	0.05N.m	0.1%
Thermocouple, k-type	Thermibel	Temperature	-200-250 °C	2.5 °C	1%
Thermocouple, k-type	Thermibel	Temperature	-200-1100 °C	10 °C	0.9%
High pressure sensor	Kistler	Pressure	0-20 bar	0.04 bar	0.2%
Incremental encoder	Lorenz	Velocity	0-1500 rpm	4.2rpm	0.28%
Flowmeter	Influx	Flowrate	1-10 L/min	0.25 L/min	2.5%
-	-	Indicated power	-	-	0.2%
-	-	Shaft power	-	-	0.3%
-	-	Thermal efficiency	-	-	2.87%

3. Thermodynamic Model

The engine is reconfigured as six cells with the expansion and compression cells considered to be adiabatic in which no heat is transferred to the surrounding. Energy is transported across the cells interfaces by means of enthalpy change in terms of mass flow and upstream temperature. As depicted in figure 3, (c, k_1, k_2, r, h, e) represent the six engine cells; compression space, connecting pipe, cooler, regenerator, heater and expansion space, respectively. While (ck_1, k_1k_2, k_2r, rh, he) represent the five interfaces between cells. The system can be regarded as quasi-steady flow by neglecting the acceleration effects of the five mass flow variables. This can reduce the problem into a set of ordinary differential equations that can be solved simultaneously. Solving these equations can be more simplified by formulating them as an initial-value problem. Due to the cyclic nature of the system, the initial values can be arbitrary defined, and then integrating the equations over several cycles until the cyclic steady state is reached. The flow chart of the developed algorithm, written in Matlab environment, is provided in figure 4.

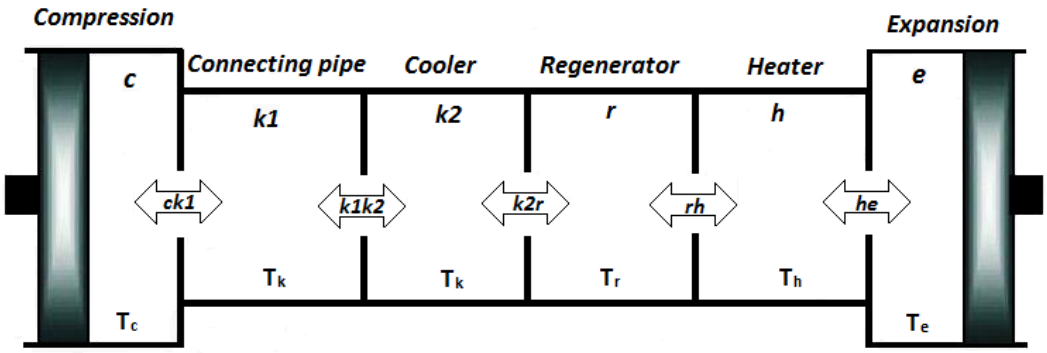

Figure 3: Schematic diagram of reconfigured adiabatic model with six engine cells.

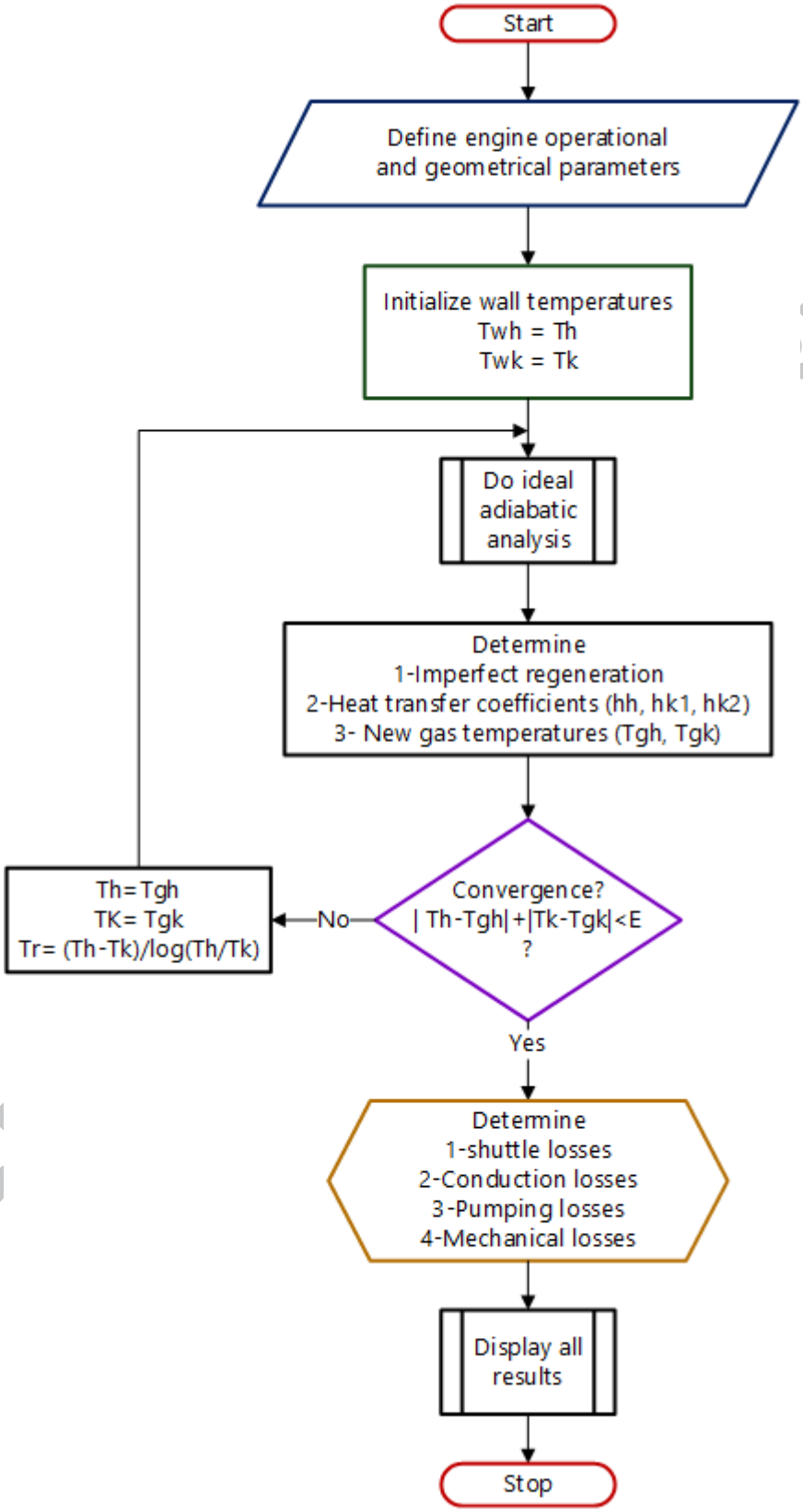

Figure 4: Flow chart of the developed algorithm.

The engine is fitted with a conventional crank mechanism. The real motion of the hot-end and cold-end pistons is adopted from [20] and can be calculated, respectively, by

$$Xe = r\left[1 - \cos\theta + \frac{1}{\lambda_e}\left(1 - \sqrt{1 - {\lambda_e}^2 \sin^2\theta}\right)\right] \quad [1a]$$

$$Xc = r\left[1 - \cos\left(\theta - \pi/2\right) + \frac{1}{\lambda_c}\left(1 - \sqrt{1 - {\lambda_c}^2 \sin^2\left(\theta - \frac{\pi}{2}\right)}\right)\right] \quad [1b]$$

Then, volume variation of expansion and compression spaces are evaluated, in terms of expansion and compression swept volumes, V_{SE} and V_{SC}, respectively, and crank radius to connecting rod ratios, λ_e and λ_c, respectively by

$$Ve = \mathrm{CVE} + \frac{V_{SE}}{2}\left[1 - \cos\theta + \frac{1}{\lambda_e}\left(1 - \sqrt{1 - {\lambda_e}^2 \sin^2\theta}\right)\right] \quad [2a]$$

$$Vc = \mathrm{CVC} + \frac{V_{SE}}{2}\left[1 + \cos\theta - \frac{1}{\lambda_e}\left(1 - \sqrt{1 - {\lambda_e}^2 \sin^2\theta}\right)\right] +$$

$$\frac{V_{SC}}{2}\left[1 - \cos\left(\theta - \pi/2\right) + \frac{1}{\lambda_c}\left(1 - \sqrt{1 - {\lambda_c}^2 \sin^2\left(\theta - \frac{\pi}{2}\right)}\right)\right] \quad [2b]$$

The pressure is assumed to be uniform throughout the engine spaces. Applying the mass conservation law to the interior spaces of the engine leads to evaluating the instantaneous engine pressure,

$$p = m\mathrm{R}/\left(\frac{V_c}{T_c} + \frac{V_{k1}}{T_k} + \frac{V_{k2}}{T_k} + \frac{V_r}{T_r} + \frac{V_h}{T_h} + \frac{V_e}{T_e}\right) \quad [3]$$

The total mass of engine gas can be calculated in terms of the charge pressure and expansion swept volume from eqn. (4) based on Schmidt theory as

$$m = \mathrm{p}_{ch} V_{SE} B\left(\sqrt{(1 + S^2)}/2RT_k\right) \quad [4]$$

Where B and S are constants dependent on geometrical and operational conditions of the engine.

The regenerator temperature is assumed to vary linearly between hot and cold end temperatures and hence can be evaluated using the logarithmic mean temperature difference as

$$T_r = (T_h - T_k)/\ln(T_h/T_k) \quad [5]$$

Applying equation of state, the mass variation through the connecting pipe, cooler, regenerator and heater are determined by

$$m_i = \frac{pV_i}{RT_i};\ i = k_1, k_2, r, h \quad [6]$$

Meanwhile, the mass accumulation in the compression and expansion cells can be determined as

$$dm_c = (pdV_c + V_c dp/\gamma)/RT_{ck1} \quad [7a]$$

$$dm_e = (pdV_e + V_e dp/\gamma)/RT_{he} \quad [7b]$$

Where, the conditional temperatures, T_{ck1} and T_{he} are dependent on the flow direction as

$$if\ \dot{m}_{ck} > 0\ then\ T_{ck1} = T_c\ else\ T_{ck1} = T_k \quad [8a]$$

$$if\ \dot{m}_{he} > 0\ then\ T_{he} = T_h\ else\ T_{he} = T_e \quad [8b]$$

Thus, the mass flow rate at each of the cells interfaces can be evaluated by

$$\dot{m}_{ck1} = -dm_c/dt \quad [9a]$$

$$\dot{m}_{k1k2} = -\dot{m}_{ck1} - dm_{k1}/dt \quad [9b]$$

$$\dot{m}_{k2r} = -\dot{m}_{k1k2} - dm_{k2}/dt \quad [9c]$$

$$\dot{m}_{rh} = -\dot{m}_{k2r} - dm_r/dt \quad [9d]$$

$$\dot{m}_{he} = -\dot{m}_{rh} - dm_h/dt \quad [9e]$$

The pressure variation is obtained from Eq. (3) as

$$dp = -\left[\frac{\gamma p[(dV_c/T_{ck1}) + (dV_e/T_{he})]}{\frac{V_c}{T_{ck1}} + \gamma(\frac{V_{k1}}{T_k} + \frac{V_{k2}}{T_k} + \frac{V_r}{T_r} + \frac{V_h}{T_h}) + \frac{V_e}{T_{he}}}\right] \quad [10]$$

The cyclic temperatures of expansion and compression spaces are calculated using the equation of state in the differential form

$$dT_i = T_i(dp/p + dV_i/V_i - dm_i/m_i);\ i = e, c \quad [11]$$

From first law of thermodynamics, the heat transfer to the cooler, regenerator and heater can be obtained as

$$dQ_k = c_v(V_{k1} + V_{k2})\frac{dp}{R} - c_p(T_{ck1}\dot{m}_{ck1} - T_k\dot{m}_{k2r}) \quad [12]$$

$$dQ_r = \frac{c_v V_r dp}{R} - c_p(T_k\dot{m}_{k2r} - T_h\dot{m}_{rh}) \quad [13]$$

$$dQ_h = \frac{c_v V_h dp}{R} - c_p(T_h\dot{m}_{rh} - T_{he}\dot{m}_{he}) \quad [14]$$

The indicated work, heat absorbed by the heater and heat rejected from the cooler can be integrated over the cycles

$$W_i = \oint p\, dV_e + \oint p\, dV_c \quad [15]$$

$$Q_k = \oint \delta Q_k \quad [16]$$

$$Q_h = \oint \delta Q_h \quad [17]$$

Since the regenerator is imperfect, the actual heat transfer to the regenerator is dependent on its effectiveness and this can be obtained using the number of transfer units, NTU of the regenerator matrix

$$\varepsilon = NTU/(1 + NTU) \quad [18]$$

The *NTU* can be determined in terms of Nusselt number, *Nu* of the regenerator matrix using the *Scaling Parameter Approach*,

$$NTU = 4Nu(lr/dr)/(RePr) \quad [19]$$

The correlations for flow friction and heat transfer in the random fibre regenerator matrix were based on oscillatory flow testing results which are presented in more detail by Geodon [21].

$$f_r = \frac{a_1}{Re} + a_2(Re)^{a_3} \quad [20a]$$

$$Nu = 1 + b_1(RePr)^{b_2} \quad [20b]$$

Thus the heat loss in the regenerator due to imperfect regeneration can be determined based on regenerator effectiveness as

$$Q_{r,loss} = (1 - \varepsilon)\left(Q_{r,max} - Q_{r,min}\right) \quad [21]$$

The actual gas temperatures in the heater and the cooler including the connecting pipe can be expressed in terms of the imperfect regeneration and heat exchange between the walls and the gas in these spaces as follows

$$Q_h = \frac{60}{n} h_h A_h (T_{wh} - T_h) - Q_{r,loss} \quad [22a]$$

$$Q_k = \frac{60}{n} (h_{k1} A_{k1} + h_{k2} A_{k2})(T_{wk} - T_k) + Q_{r,loss} \quad [22b]$$

The heat transfer coefficients in heater, connecting pipe and cooler, h_h, h_{k1} and h_{k2}, respectively are based on Colburn J-factor found in Kays and London [22]

$$J = hPr^{2/3}/(\dot{m}C_p/A_f) \quad [23a]$$

Where,

If Re < 3000

$$J = \exp(0.337 - 0.812\log(Re)) \quad [23b]$$

If 3000<Re< 4000

$$J = 0.0021 \quad [23c]$$

If 4000<Re<7000

$$J = \exp(13.31 - 0.861\log(Re)) \quad [23d]$$

If 7000<Re<10000

$$J = 0.0034 \quad [23e]$$

If Re>10000

$$J = \exp(-3.575 - 0.229\log(Re)) \quad [23f]$$

The internal conduction losses in the regenerator and the shuttle losses due to oscillatory motion of the displacer are included to calculate the actual heat transferred to the heater

$$Q_{d,loss} = \frac{k_r A_r}{l_r}(T_h - T_k) \quad [24a]$$

$$Q_{sh,loss} = \frac{0.4 {Z_d}^2 k_d D_d}{J_d l_d}(T_e - T_c) \quad [24b]$$

$$Q_{act,h} = Q_h + Q_{d,loss} + Q_{sh,loss} \quad [24c]$$

The work loss due to pressure drop in connecting pipe, cooler, regenerator and heater can be obtained by

$$W_{loss} = \oint \Delta p_i \, dV_e \quad [25]$$

The pressure drop for all heat exchangers can be expressed by an equation that satisfies the momentum conservation for positive and reversed flow such as

$$\Delta p_i = -2 f_r \mu u \left(\frac{V_i}{A_i {d_i}^2}\right); \; i = k_1, k_2, r, h \quad [26a]$$

The Reynolds friction factor, f_r, can be determined from Darcy friction factors and Reynolds number.

$$f_r = \left(\frac{f_D}{4}\right) Re \quad [26b]$$

Eqn.(20a) is used to quantify the pressure drop in the regenerator, while, the pressure drop in connecting pipe, cooler and heater is determined using friction factor evaluated by [23]

If Re < 2000

$$f_D = \frac{64}{Re} \quad [27a]$$

If 2000 < Re < 20000

$$f_D = 0.316Re^{-0.25} \quad [27b]$$

If Re >20000

$$f_D = 0.184Re^{-0.2} \quad [27c]$$

The forced work per cycle, $\bar{W}$, shown in figure 5, can be evaluated by integrating the product of (p-p_{ch}) and dV over the portions of the cycle but with negative sign.

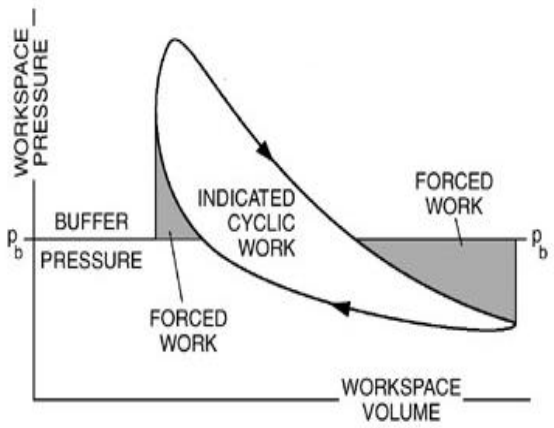

Figure 5: Schematic diagram of forced work.

$$\bar{W} = \oint [(p - p_{ch})\, dV]^{-} \quad [28]$$

The engine shaft work per cycle W_s can then be calculated in terms of the indicated work and the forced work based on Senft's theory [24] as,

$$W_s = E(W_i - W_{loss}) - (1/E - E)\bar{W} \quad [29]$$

Where, E is the mechanism effectiveness. For a heat engine, the mechanical effectiveness typically varies between 0.7 and 0.9. In present work, the mechanism effectiveness of the engine is calibrated to experiment and found to be 0.75. the shaft power of the engine ($\dot{W}_s$) can be obtained in terms of the shaft work and the engine speed as.

$$\dot{W}_s = W_s\left(\frac{n}{60}\right) \quad [30]$$

Similarly, the engine torque can be expressed as

$$\tau = \left(\frac{\dot{W}_s}{\omega}\right) \quad [31]$$

Finally, the thermal efficiency of the engine, can be calculated in terms of the shaft power and the actual heat input as

$$\eta_{th} = \left(\frac{\dot{W}_s}{\dot{Q}_{act,h}}\right) \quad [32]$$

4. Model validation

In this section, a comparison of the results of the simulated engine and experiment are presented. The operational conditions of the engine were listed previously in table 1. The indicated PV diagrams are compared to experiment at the two extremes of hot end temperatures and charge pressures as shown in figure 6 and 7 at engine nominal speed.

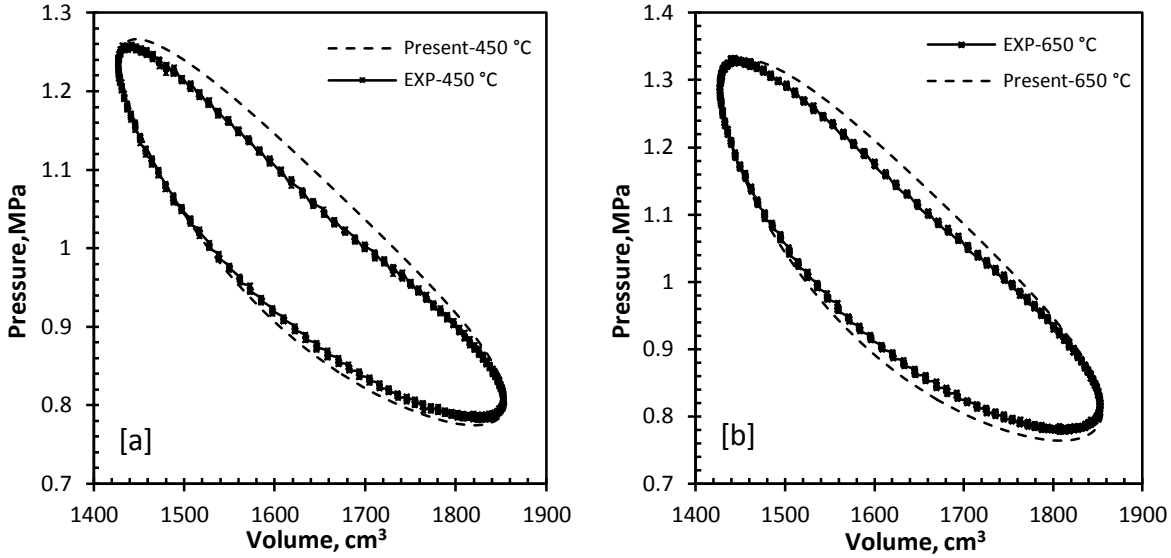

Figure 6: Comparison of indicated PV diagrams of N2 between the present model and experiment at Fixed charge pressure (10bar) and different heater temperatures, (a) at 450 °C and (b) at 650 °C.

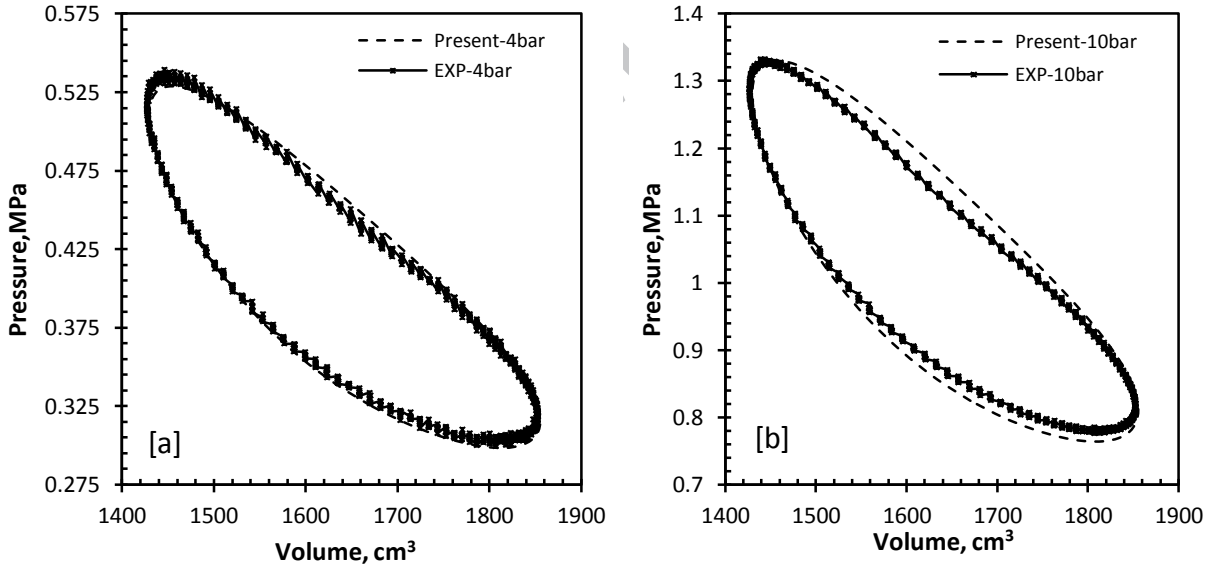

Figure 7: Comparison of indicated PV diagrams of N2 between the present model and experiment at Fixed heater temperature (650 °C) and different charge pressures, (a) at 4 bar and (b) at 10 bar.

It can be seen that the minimum and the maximum pressures predicted by the model are very similar to experimental results. This suggests that calculating the instantaneous pressure based on gas equation of state is reasonably accurate. However, the gap areas in indicated PV diagrams between model experimental results are observed. The indicated PV diagram obtained from experiment is based on actual pressure drop in all spaces of the engine. Meanwhile, the pressure drop in the current model is decoupled from the indicated PV diagram and added in the final evaluation of engine performance. In general, the

maximum deviation in predicting the indicated power is 15% compared to experimental results observed at lower hot end temperature.

In figure 8, a comparison between model and experimental results in predicting shaft power and engine thermal efficiency at different hot end temperatures is presented. As can be seen, power increases with increasing the hot end temperature. The maximum shaft power reads 470 W at 500 rpm for both model and experimental results at the maximum hot end temperature of 650 °C. In general, the shaft power is over-predicted with a maximum deviation of 15% which occurs at lower hot end temperature of 450 °C. For engine efficiency, the trend is similar with a maximum value of 16.9 % achieved at maximum hot end temperature of 650 °C. A 7.5 % maximum deviation is depicted at lower hot end temperature.

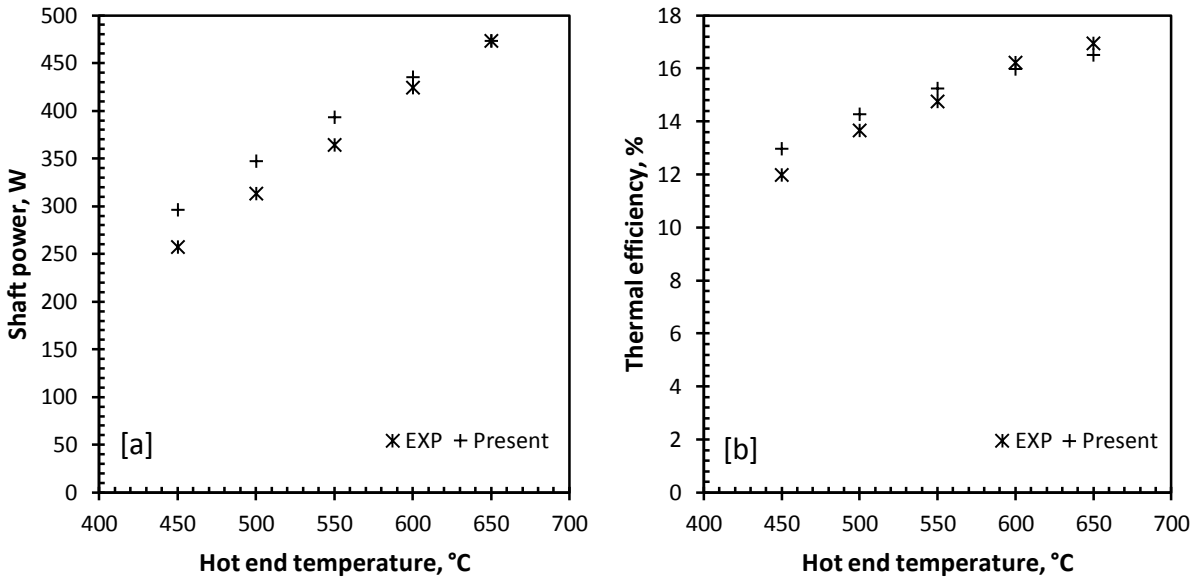

Figure 8: Comparison of N2 results between the present model and experiment at constant charge pressure (10bar) and different heater temperatures, (a) shaft power and (b) engine efficiency.

In figure 9, the shaft power predicted at different charge pressures are very similar to the experimental results. In terms of thermal efficiency, the trend is similar to experiment. However, efficiency is over-predicted with a maximum deviation of 8% which occurs at charge pressures of 7 and 8 bar. This may be attributed to the uncertainty in measuring the flow rate and inlet and outlet cooling temperatures, which in had affected the calculation of thermal efficiency, accordingly.

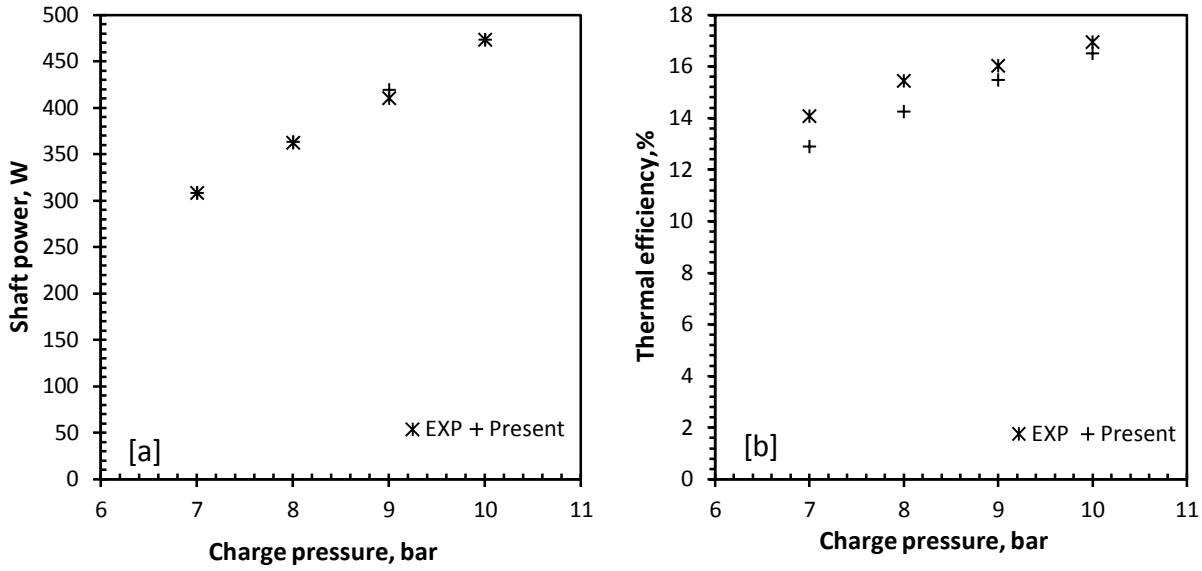

Figure 9: Comparison of N2 results between the present model and experiment at constant heater temperature (650 °C) and different charge pressures, (a) shaft power and (b) engine efficiency.

Figure 10 compares the predicted shaft power with experiment at different engine speeds and two extreme hot end temperatures. It can be found that with increasing the speed, the shaft power reaches to its maximum at an optimum speed and then falls down. This is attributed to that pressure drop is more pronounced at higher speeds due to elevated frictional losses. The optimum speed, predicted and from experiment, is very similar which reads 600 rpm at hot end temperature of 650 °C compared to 500 rpm at hot end temperature of 450°C.

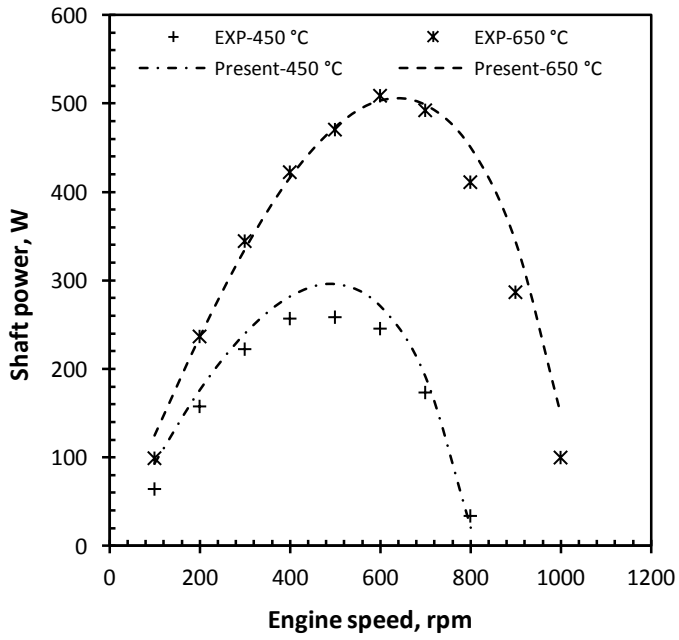

Figure 10: Comparison of N2 results of shaft power versus engine speed between the present model and experiment at constant charge pressure (10bar) and different heater temperatures (450 °C and 650 °C).

5. Results and discussion

Once the model was validated with experiment, a parametric study was carried out to investigate the effect of phase angle, matrix type, gas type and low cooling temperature on engine performance.

5.1 Effect of phase angle

In most gamma-type Stirling engines, the phase angle can be adjusted for maximum shaft power based on the operating conditions. The optimum phase angle is usually assumed to be 90° for practical purposes [25]. However, the results shown in figure 11, shows that maximum shaft power of 525 W occurs at phase angle of 100° compared to 503 W at angle of 90°. On the other hand, maximum thermal efficiency is still near at 90° angle.

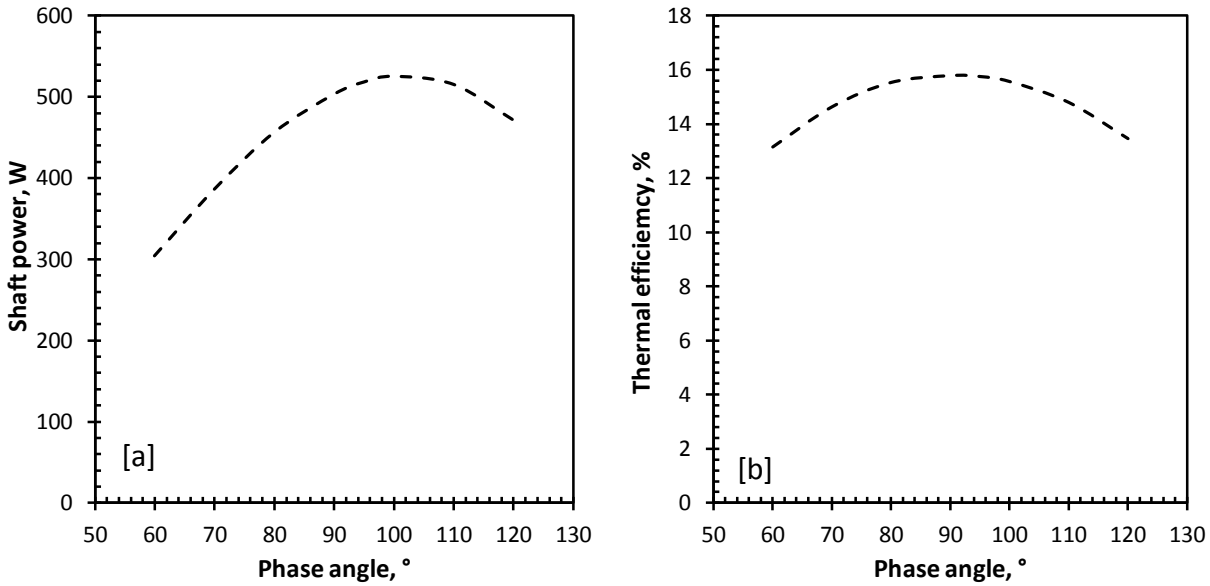

Figure 11: Effect of phase angle on engine performance, (a) shaft power and (b) engine efficiency.

5.2 Effect of matrix type

The engine is originally fitted with random fibre regenerator (type 3). Three configurations, listed in table 3, were investigated.

Table 3: Random fibre configurations

Type	Commercial name	Wire diameter, μm	Porosity, %	Material
1	1 mil Brunswick	27.4	82	stainless steel
2	12 micron Bekaert	13.4	89.7	stainless steel
3	31 micron Bekaert	31	90	stainless steel

The difference in engine performance using different regenerator fillings is demonstrated in figure 12. Both shaft power and thermal efficiency increased with engine speed till the optimum speed for all configurations. It can be seen that type 3 is superior to type 1 and type 2, with shaft power produced 503W, 316 W and 255W, respectively. Type 1 has the highest wire diameter and porosity so that the heat transfer rate is increased due to the increased surface area. This explains why the shaft power is increased when using type 3. On the other hand, type 1 combines moderate wire diameter and porosity. The optimum speed occurs when the negative effects of elevated pressure drop is balanced with the positive effects of increased heat transfer. The optimum speed for type 2, type 1 and type 3 occurs at 400 rpm, 500 rpm and 600 rpm, respectively. For the thermal efficiency, the optimum speed occurs at 300 rpm, 400 rpm and 500 rpm for type 2, type 1 and type 3, respectively.

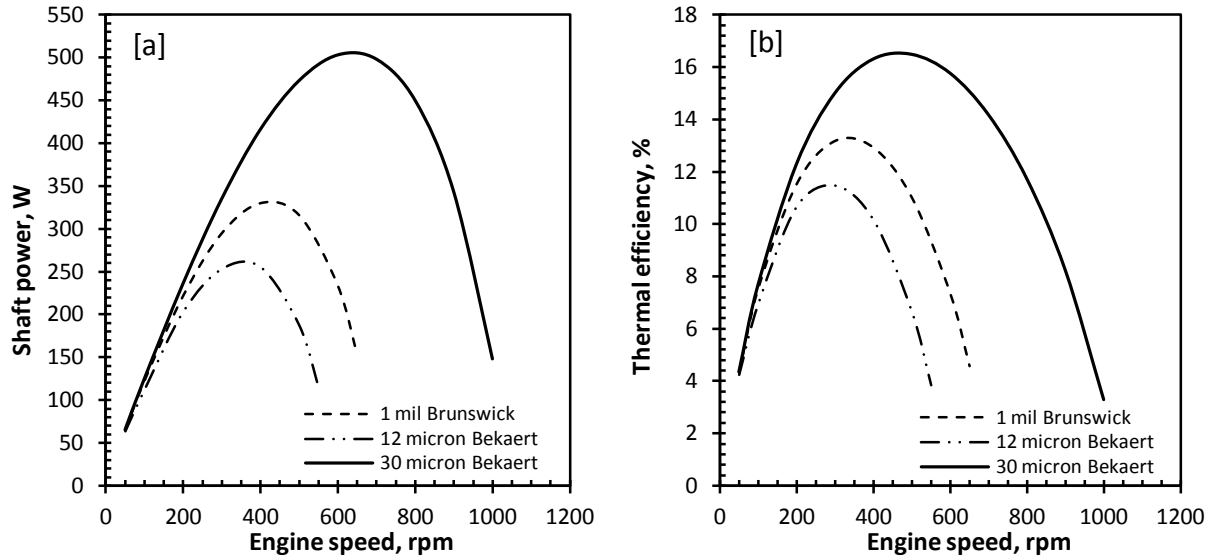

Figure 12: Effect of regenerator matrix on engine performance, (a) shaft power and (b) engine efficiency.

5.3 Effect of gas type

Most developed Stirling engines can run fast when charged with helium than with air [26]. Helium possesses higher power density due to its low viscosity and higher thermal conductivity. In this regard, the effect of gas type on engine performance at different engine speeds was presented in figure 13. The charge pressure and hot end temperature were maintained at their maximum values of 10 bar and 650 °C, respectively. It is observed that when helium is used, the shaft power exhibits superior values than nitrogen at higher engine speeds. Up to speed of 500 rpm, no significant difference of shaft power is observed between the two gases. At 1100 rpm engine produces maximum power of 712 W when using helium compared to 503 W at 600 rpm when using nitrogen. The thermal efficiency drops steeply from 16.5% to 3% when using nitrogen between 500 to 1000 rpm. Meanwhile, thermal efficiency using helium drops steadily from 16.3% to 8.4% between 700 to 1500 rpm.

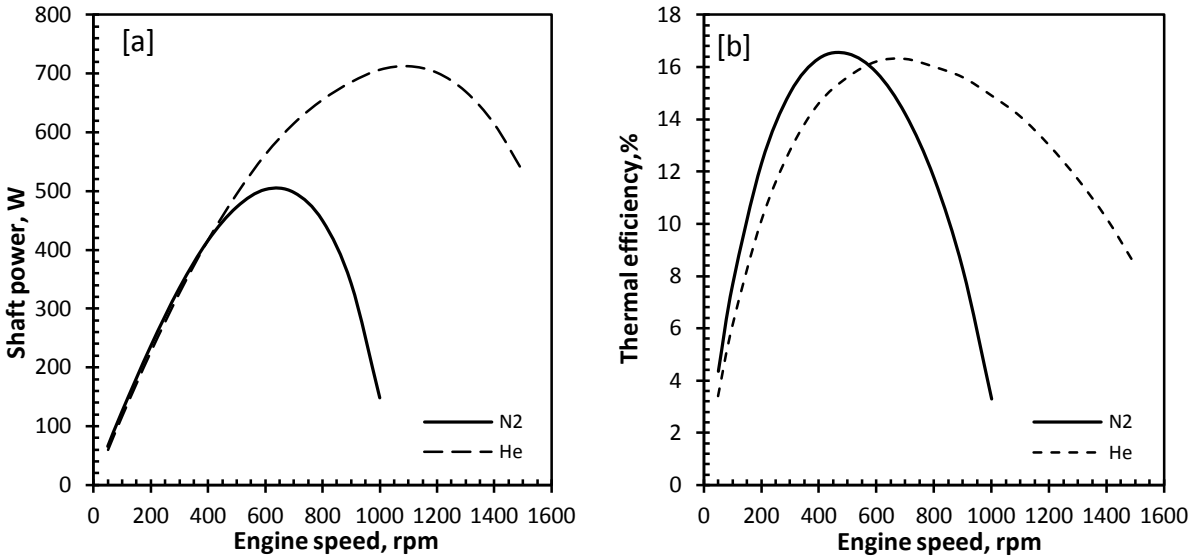

Figure 13: Effect of gas type on engine performance, (a) shaft power and (b) engine efficiency.

5.4 Effect of low temperature cooling

Cryogenic fluids including liquid air/LN2 have been acknowledged as energy storage vectors with high storage density of 0.77 [MJ/kg]. Surplus electricity (off-peak) and/or the renewable energy sources can be used to liquefy air/N2 in which can be stored and transported using the well-developed cryogenic industry infrastructure. In this work, the feasibility of utilizing the stored cold energy of LN2 to maximize the shaft power of the engine was investigated. Figure 14 shows the effect of low cooling temperature, in the range of (15 ˚C to -150 ˚C), on the shaft power and thermal efficiency for nitrogen and helium as working gases. In all figures [a, b, c and d], both shaft power and thermal efficiency increase with lowering the cooling temperature for helium and nitrogen. As cooling temperature decreases, the minimum cyclic pressure is reduced giving rise to the average cyclic pressure thus producing higher power density. Similarly shaft power and thermal efficiency is increased when hot end temperature is increased from 450 ˚C to 650 ˚C. As heating temperature is increased from 450 ˚C to 650 ˚C, a 49% enhancement of shaft power is achieved for helium at -50 ˚C reaching 1kW and 35% for Nitrogen reaching 700 W. This compares to a 35% enhancement of thermal efficiency for helium at -50 ˚C reaching 18.8% and 23% enhancement for Nitrogen reaching 19.7% when compared to that at normal cooling temperature of 15 ˚C.

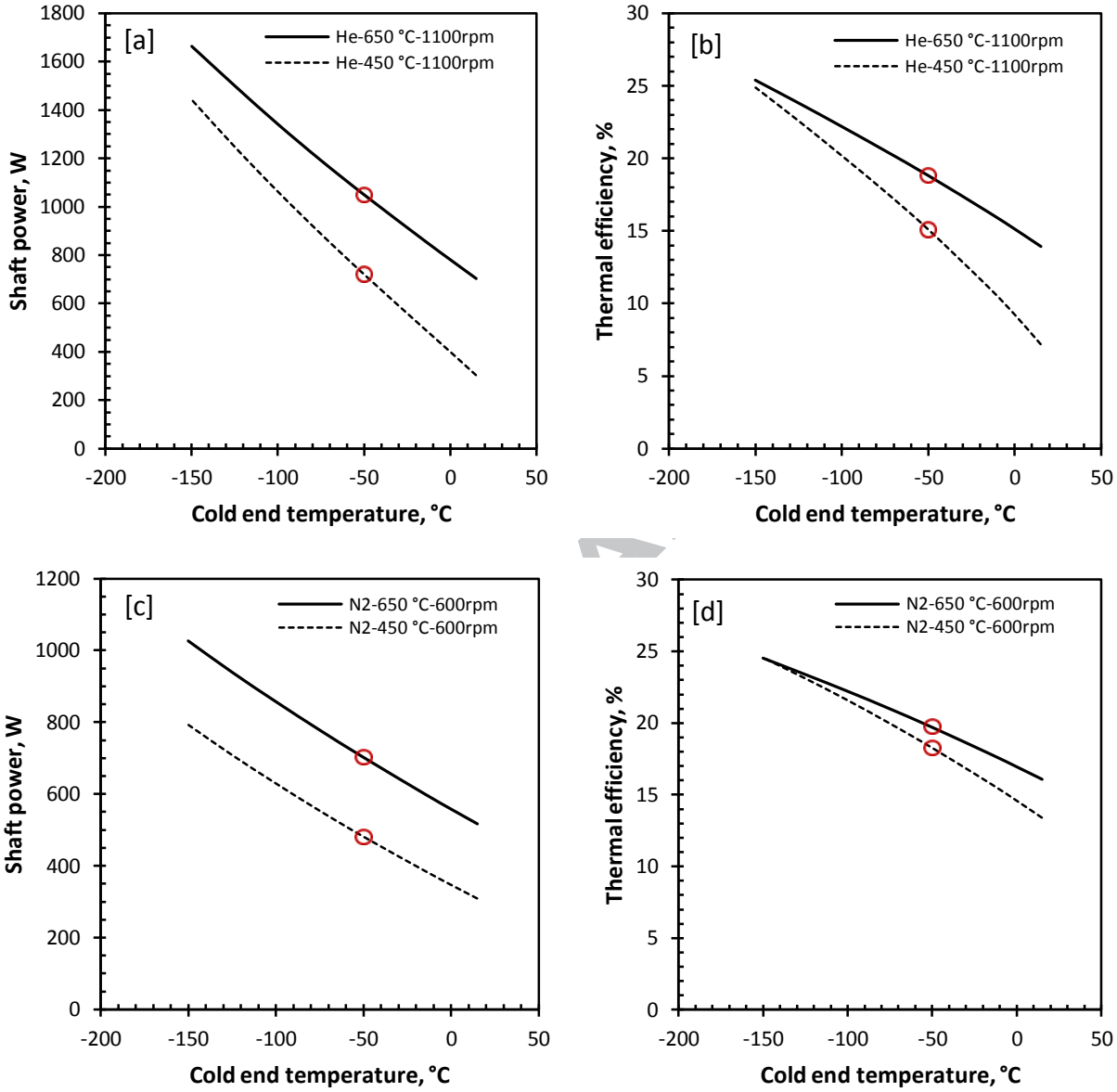

Figure 14: Effect of cold end temperature on engine performance at different hot end temperatures for helium (a, b) and nitrogen (c, d).

5.5 Effect of dead volume

The dead-volume of the connecting pipe can be reduced to enhance the engine performance [27]. The effect of pipe diameter, connecting both parts of the compression space, on N2-charged engine performance was illustrated in figure 15. It can be seen that as pipe diameter is reduced, from 30 mm to 15mm, the dead volume is reduced by 50%, the shaft power is enhanced by 20% reaching a maximum of

623 W at pipe diameter of 16 mm. The thermal efficiency is similarly enhanced by 5% reaching 16.9% but at different optimum diameter of 20 mm.

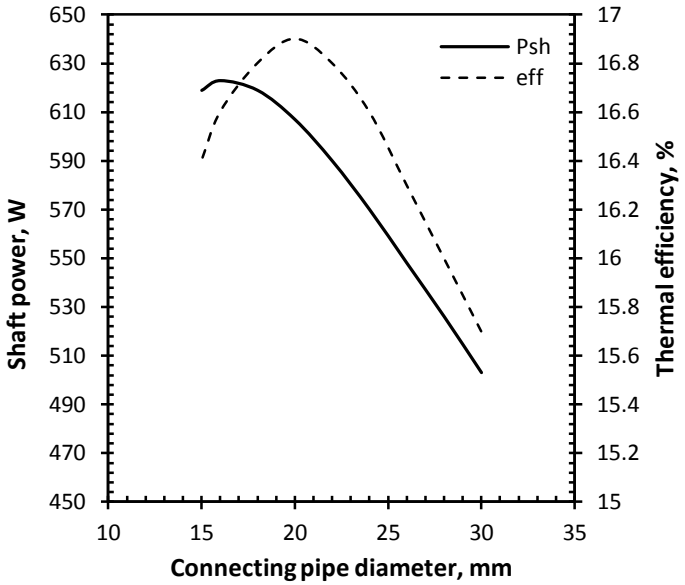

Figure 15: Effect of cold end temperature on engine performance at different hot end temperatures, (a) shaft power and (b) engine efficiency.

6. Conclusion

An enhanced thermodynamic model based on non-ideal adiabatic analysis, is developed to simulate gamma-type Stirling engine (ST05-CNC). The engine is reconfigured with six engine cells to include the connecting pipe for better accuracy. Random fibre correlations for flow friction and heat transfer, based on oscillatory flow testing were used to model the regenerator. The real pistons motion was adopted and hence the real volume variation was included in the model. The pumping losses in the heat exchangers were evaluated depending on the type of flow regime. Thermal losses such as shuttle and conduction losses are accounted for as well as the mechanical losses to estimate the shaft power. A maximum deviation of 15% was found between model and experimental results. The maximum deviation of the model prediction is lower than that of some published work with similar methodology and analysis.

The model was further used to investigate the effect of phase angle, gas type, regenerator matrix type, dead volume and low cooling temperature on engine performance. A 20% enhancement in shaft power was achieved as the connecting pipe diameter was reduced by a 50%. This is in a good agreement with a previously published work on a gamma-type Stirling engine. Also, the low cooling effect on shaft power

is addressed in this work and the shaft power was found to be significantly enhanced by 49% for helium and 35% for nitrogen when cooling temperature is lowered to -50 °C while heating temperature remains constant at 650 °C.

The theoretical results obtained from the model, (helium as a working gas, connecting pipe reduction, and phase angle adjustment), will be verified with further experimental testing to demonstrate the impact of engine improvements on its performance.

References

[1] Goswami DY, Kreith F, editors. Handbook of energy efficiency and renewable energy. Crc Press; 2007.

[2] Organ, AJ. The air engine: Stirling cycle power for a sustainable future. Elsevier, 2007.

[3] Walker G. Stirling engines. Oxford University Press; 1980.

[4] Ibrahim MB, Tew Jr RC. Stirling convertor regenerators. CRC Press; 2011.

[5] Thombare DG, Verma SK. Technological development in the Stirling cycle engines. Renewable and Sustainable Energy Reviews. 2008;12(1):1-38.

[6] Beale WT, Wood JG, Chagnot BF. Stirling engine for developing countries. American Institute of Aeronautics and Astronautics 1980; 809399:1971–5.

[7] West CD. A fluidyne Stirling engine, report no. AERE-R 6776. Harwell University; 1981.

[8] Schmidt G. Classical analysis of operation of Stirling engine. A report published in German Engineering Union (Original German), vol. XV; 1871. p. 1–12.

[9] Organ AJ. Back to back test for determining the pumping losses in Stirling cycle machine. Proceedings of the ^{17}th intersociety energy conversion engineering conference, 1982. p. 1856–61.

[10] Urieli I, Berchowitz DM. Stirling cycle engine analysis. Taylor & Francis; 1984.

[11] Finkelstein T. Generalized thermodynamic analysis of Stirling cycle engines. SAE paper no. 118A, 1960.

[12] Martini WR. Stirling engine design manual. Richland (USA): Washington Univ., Joint Centre for Graduate Study; 1978.

[13] Timoumi Y, Tlili I, Nasrallah SB. Design and performance optimization of GPU-3 Stirling engines. Energy 2008;33(7):1100–14.

[14] Cheng CH, Yang HS, Keong L. Theoretical and experimental study of a 300-W beta-type Stirling engine. Energy 2013; 59:590–9.

[15] Babaelahi M, Sayyaadi H. Simple-II: a new numerical thermal model for predicting thermal performance of Stirling engines. Energy 2014; 69:873–90.

[16] Hosseinzade H, Sayyaadi H. CAFS: the combined adiabatic–finite speed thermal model for simulation and optimization of Stirling engines. Energy Convers Manage 2015; 91:32–53.

[17] Hosseinzade H, Sayyaadi H, Babaelahi M. A new closed-form analytical thermal model for simulating Stirling engines based on polytropic-finite speed thermodynamics. Energy Convers Manage 2015; 90:395–408.

[18] Ve-ingenieure. Datasheet ST05-G Striling engine. 2015 [online]: http://www.ve ingenieure.de/projekt_st05g_cnc_engl.html

[19] Moffat RJ. Describing the uncertainties in experimental results. Experimental Thermal and Fluid Science 1988;1(1):3-17.

[20] Wagner A. Calculations and experiments on gamma-type Stirling engines. Cardiff University; 2008.

[21] Gedeon D, Wood JG. Oscillating-flow regenerator test rig: hardware and theory with derived correlations for screens and felts; 1996.

[22] Kays WM, London AL. Compact heat exchangers. Krieger Pub Co; 1998.

[23] Incropera FP, DeWitt DP. Fundamentals of heat and mass transfer. John Wiley, 2007.

[24] Senft JR. An introduction to Stirling engines. USA: Moriya Press; 2004.

[25] Senft JR. Optimum Stirling engine geometry. Int. J Energy 2001; 1:1087–101.

[26] Walker M. Stirling cycle machines. Oxford: Clarendon Press; 1973.

[27] Mahkamov K. Design improvements to a biomass Stirling engine using mathematical analysis and 3D CFD modelling. Journal of Energy Resources Technology. 2006;128(3):203-15.

Highlights

- Enhanced thermodynamic model for gamma-type Stirling engine was developed.
- Validation against experiments was performed.
- Influence of different parameters on engine performance was investigated.
- Deeper insight into engine improvements was highlighted.
- Effect of low temperature cooling on engine performance was addressed.